Earth and Planetary Science Letters ••• (••••) ••••••

Contents lists available at ScienceDirect

Earth and Planetary Science Letters

www.elsevier.com/locate/epsl

Geochemical evidence of Milankovitch cycles in Atlantic Ocean ferromanganese crusts

Pierre Josso [a,*], Tim van Peer [b], Matthew S.A. Horstwood [a], Paul Lusty [a], Bramley Murton [c]

[a] British Geological Survey, Environmental Science Centre, Keyworth, Nottingham NG12 5GG, UK
[b] University of Southampton, Waterfront Campus, European Way, Southampton SO14 3ZH, UK
[c] National Oceanography Centre, Waterfront Campus, European Way, Southampton SO14 3ZH, UK

ARTICLE INFO

Article history:
Received 16 March 2020
Received in revised form 19 August 2020
Accepted 26 October 2020
Available online xxxx
Editor: L. Robinson

Keywords:
Fe-Mn crust
Pb isotopes
astronomical parameters
astronomical tuning
ITCZ
West African Craton

ABSTRACT

Hydrogenetic ferromanganese crusts are considered a faithful record of the isotopic composition of seawater influenced by weathering processes of continental masses. Given their ubiquitous presence in all oceans of the planet at depths of 400–7000 meters, they form one of the most well-distributed and accessible records of water-mass mixing and climate. However, their slow accumulation rate and poor age constraints have to date limited their use to explore 100 ka paleoclimatic phenomena. Here it is shown how the Pb isotope signature and major element content of a Fe-Mn crust from the north-east Atlantic responded to changes in the intensity and geographic extent of monsoonal rainfall over West Africa, as controlled by climatic precession during the Paleocene. The studied high-spatial resolution (4 μm) laser-ablation multi-collector inductively coupled plasma mass spectrometer (LA-MC-ICP-MS) Pb isotope data is a nearly 2 order of magnitude improvement in spatial and temporal resolution compared to micro-drill subsamples. The record demonstrates cyclicity of the $^{206}Pb/^{204}Pb$ and $^{208,207}Pb/^{206}Pb$ ratios at the scale of single Fe-Mn oxide laminae, in conjunction with variations in the Fe/Mn ratio, Al, Si and Ti content. Time-frequency analysis and astronomical tuning of the Pb isotope data demonstrates the imprint of climatic precession (~20 ka) modulated by eccentricity (~100 and 405 ka), yielding growth rates of 1.5–3.5 mm/Ma consistent with previous chemostratigraphic age models. In this context, boreal summer at the perihelion causes stronger insolation over West Africa, resulting in more intense and geographically extended monsoonal rainfalls compared to aphelion boreal summer conditions. This, in turn, influences the balance between the weathering endmembers feeding the north-east Atlantic basin. These results provide a new approach for calibrating Fe-Mn crust records to astronomical solutions, and allow their isotopic and chemical archive to be exploited with an improved temporal resolution of 1000–5000 years.

1. Introduction

Astronomical parameters are one of the major drivers of climate on timescales of 10^4–10^5 years. These result in high-frequency variations superimposed on long-term changes controlled by tectonic processes (10^6 years) (Zachos et al., 2001). Quasi-periodic oscillations in Earth's astronomical parameters, comprising precession (the wobbling movement of Earth's rotational axis), obliquity (the tilt of Earth's rotational axis) and eccentricity (the shape of Earth's orbit around the sun) affect the distribution and amount of solar energy received by the atmosphere.

The development of the astronomical theory allowed prediction of prevailing paleoclimate conditions in the geological past, with major importance to the fields of anthropology, including studying the impact of African climate on hominid evolution and migration (Bonnefille, 2010). Numerous models have been produced to show how climate in this region has evolved due to changes in the position and intensity of the tropical rain belt over North Africa. The extent of the topical rain belt in this region is affected by changes in the average position of the Intertropical Convergence Zone (ITCZ), as a result of precession-induced high or low insolation conditions occurring about every 20 ka (Tierney et al., 2011; Skonieczny et al., 2015; Liu et al., 2019). High-temporal resolution palynological and sedimentological records from African lakes and offshore records demonstrate the regular alternation of dryer and wetter climates over northern Africa (Abouchami and Zabel, 2003; Tierney et al., 2011). Here it is reported how deep-oceanic hydrogenetic ferromanganese (Fe-Mn) crusts record information on astronomically induced hydroclimatic change over North Africa

* Corresponding author.
E-mail address: piesso@bgs.ac.uk (P. Josso).

https://doi.org/10.1016/j.epsl.2020.116651

during the Paleocene and inform on the weathering regime present during this period.

Since the 1990's, deep-sea hydrogenetic Fe-Mn crusts have been used for long-term (resolution ~0.5 Ma) paleoceanographic reconstructions (Abouchami et al., 1997; Christensen et al., 1997). These reconstructions rely on using a variety of radiogenic isotopes (e.g. Nd, Hf, Pb) to decipher water-mass provenance and mixing through time, and the intensity and source of weathering inputs from continental environments (Frank et al., 1999; Reynolds et al., 1999; Frank et al., 2002; Van De Flierdt et al., 2003). Fe-Mn crusts form by the extremely slow accumulation (few mm per million years; mm/Ma) of highly reactive Fe and Mn oxyhydroxide colloids on indurated substrates in the ocean (Lusty et al., 2018). These characteristics result in the Fe and Mn oxide layers scavenging dissolved trace metals from seawater, which means they form condensed archives of paleo seawater composition influenced by the weathering inputs from continental masses, aerosols and hydrothermal sources (Koschinsky and Hein, 2017). The main limitations in the application of these records are the reliability of age-models over the Cenozoic, which are derived from a variety of radiogenic (Be, Os, Th) measurements, biostratigraphic analysis and empirical methods (Co-chronometers), and their poor-temporal resolution as a result of the very slow accumulation rates (Josso et al., 2019).

A link between astronomical parameters and changes in the primordial texture and geochemistry of Fe-Mn nodules was suggested by Han et al. (2003) whilst glacial-interglacial variations in Pb isotopes data were highlighted previously (Abouchami et al., 1997; Christensen et al., 1997). However, the detailed mechanism by which changes in astronomical parameters were transferred to marine Fe-Mn oxides was not conclusively established because of the variety of potential environmental influences on chemical variability in Fe-Mn crusts (latitudinal migration, depth variation, bioproductivity, oceanic currents) (Mizell et al., 2020). A further challenge for assessing the influence of astronomical parameters on Fe-Mn crust composition is the limited sampling resolution of traditional micro-drilling method of these deposits, and uncertainty in dating. In this study, laser-ablation multi-collector inductively coupled plasma mass spectrometry (LA-MC-ICP-MS) was used to acquire Pb isotope data at a high spatial-resolution of 4 µm, which represents an improvement of two orders of magnitude compared to a continuous 500 µm micro-drilling study. This temporal resolution makes it possible to unequivocally investigate the imprint of the astronomical parameters. Lead isotopes in marine records have previously been shown to correlate closely with climate variations over the last 7 Ma (Christensen et al., 1997; Gutjahr et al., 2009), and be free of influence from stochastic geochemical variations. The data presented here demonstrate that marine ferromanganese precipitates recorded the different weathering input from West Africa as a result of latitudinal migration and intensity variation of the tropical rain belt controlled by astronomical parameters.

2. Materials and methods

The Fe-Mn crust sample 085_004 used in this study was obtained from Tropic Seamount (23° 53.77 N, 20° 46.06 W), 450 km from the coast of West Africa, at a water depth of 1130 metres below sea level, during the JC142 expedition, which formed part of the "MarineE-Tech" research project (Fig. 1). A remotely operated vehicle (ROV) mounted-drill produced a 20 cm long core by drilling through a Fe-Mn crust pavement. This comprised 15 cm of layered Fe-Mn oxides, sitting on top of a phosphatised, biogenic debris-rich carbonate substrate (Fig. 1, Josso et al. (2020b)). Ages were derived using Bayesian statistical modelling of Markov Chain Monte Carlo simulations employing a combination of Co chronometry, Os isotopes and U-Pb dating as the constraining parameters (Josso et al., 2019). The Fe-Mn crust initiated its growth in the Late Cretaceous (75 ± 2 Ma), followed by alternating periods of growth and erosion (Fig. 1). Another study (Josso et al., 2020a) explored the long-term Pb and Nd isotopic variations of this sample over the last 75 Ma in the context of an evolving oceanic basin and climate throughout the Cenozoic. The present investigation focuses in high-detail on a 7 mm stratigraphic interval (125–118 mm from the top of the sample), selected because of optimal temporal and textural control (Fig. 2). This stratigraphic interval spans the early Paleocene and its age is constrained between 65.1 ± 0.7–63.0 ± 0.6 Ma (Josso et al., 2019) (2σ precision). Well-defined alternating laminated and columnar horizons (Fig. 2) are present in this interval, with traceable individual oxide laminae across the area of data acquisition, thereby providing a strong stratigraphic and spatial control on the data collected (Fig. 2).

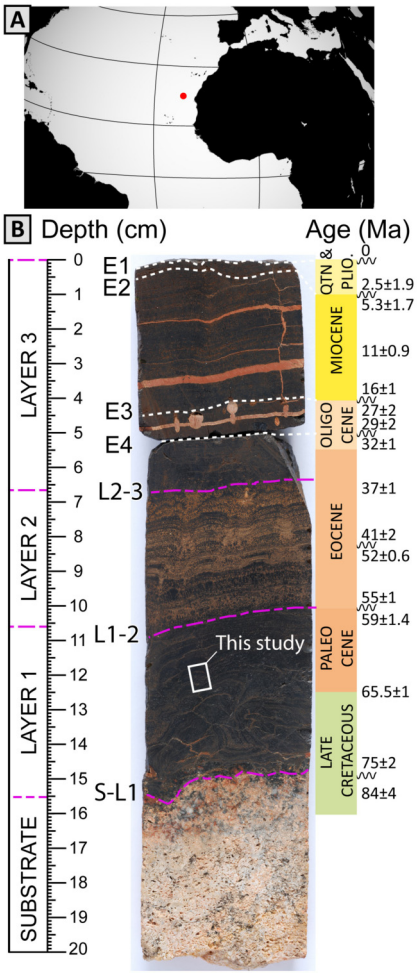

Fig. 1. (A) Location of Tropic Seamount in the north-east Atlantic. (B) Cut section of core 085_004 showing the presence of three Fe-Mn oxide macro-layers resting on a carbonate substrate (modified from Josso et al. (2020b)). The white rectangle highlights the zone of interest for this study. An electron-back-scatter map of this area is presented in Fig. 2. See Josso et al. (2019) for details on establishment of the age model and Josso et al. (2020b) for a complete description of the geochemistry and textures of the core. (For interpretation of the colours in the figure(s), the reader is referred to the web version of this article.)

All measurements were carried out on a 100 µm thick polished thin section of the sample. Backscatter electron imaging and energy dispersive X-ray measurements for elemental distribution were performed on an FEI Quanta 600 scanning electron microscope (SEM) fitted with an Oxford Instruments INCA Energy 450 X-ray microanalysis system. Elemental mapping was performed

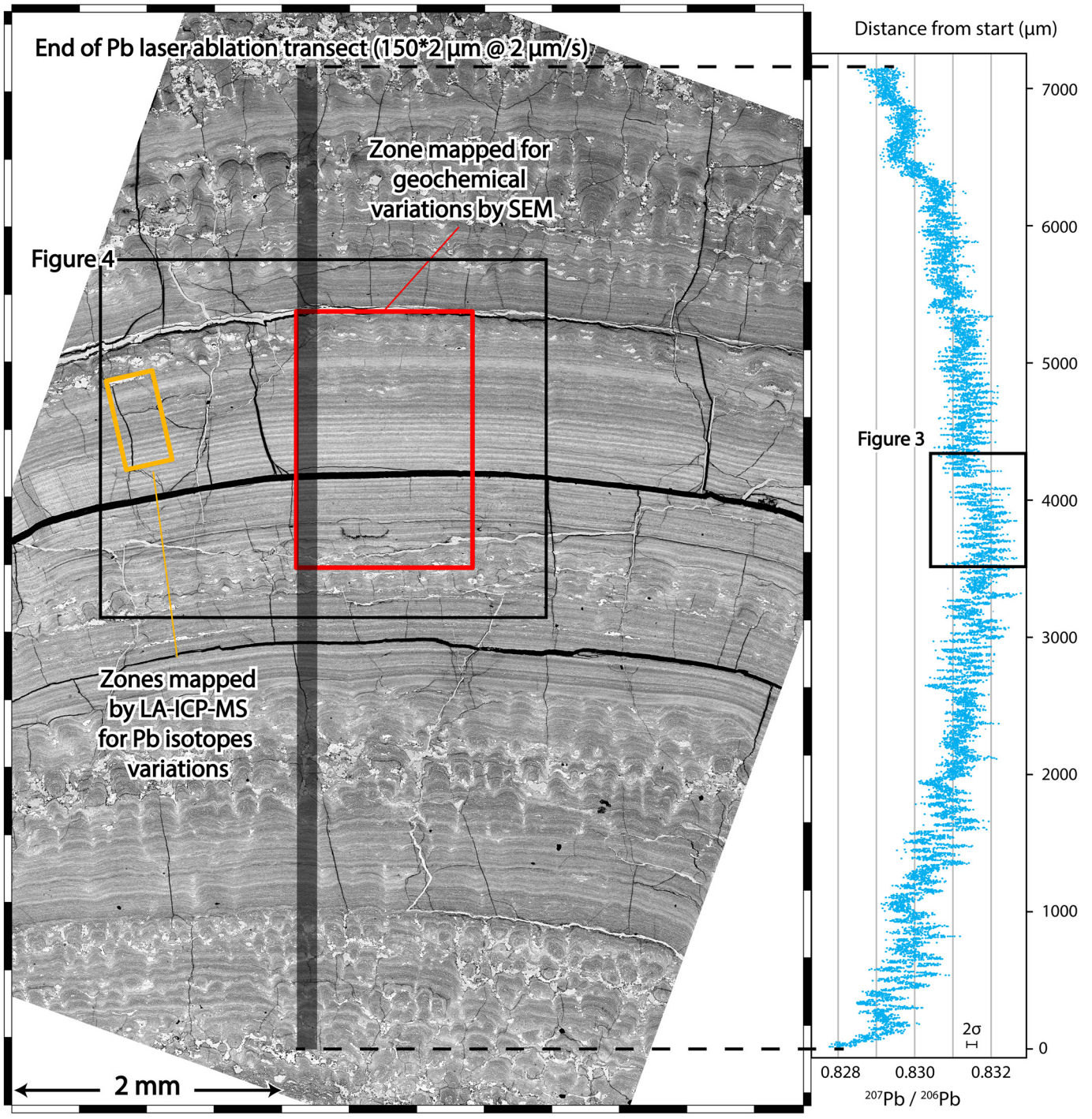

Fig. 2. Backscatter electron microscope image of the area studied in sample 085_004 showing intervals of laminar Fe-Mn oxides alternating with a columnar texture in which the intercolumnar space is filled by carbonate-fluoro-apatite (Josso et al., 2020b). The transect and zones analysed for Pb isotopes by LA-MC-ICP-MS and phase mapping by SEM are shown in the overlay. The black rectangles represent the zones shown in Figs. 3 and 4. The $^{207}Pb/^{206}Pb$ ($\pm 0.015\%$, 2σ) isotope profile used for cyclostratigraphy is shown on the right hand side. The complete dataset is available in supplementary information (DOI: https://doi.org/10.5285/7a9eb43f-a5c4-450c-9fe1-c60f2703a1d1).

with a 20 kV acceleration voltage and a 10 mm working distance. Twenty-eight areas with ~20% spatial overlap were collected at beam currents of ~2 nA with INCA process time 3, for a total of ~50 million counts per field of view. Areas were stitched together using the INCA Montage module. Phase distributions, principally defined by variations in Fe/Mn ratios, were obtained using the INCA PhaseMap module and individual element distribution maps are contained in the Supplementary Material 1.

Pb isotope data were acquired using LA-MC-ICP-MS on the thin section. An Elemental Scientific Lasers NWR193UC laser ablation system was coupled to a ThermoScientific Neptune Plus MC-ICP-MS. Data were acquired in continuous transects using a letterbox format ($2 * 150$ µm) ablation spot rastering perpendicular to the sample layering at 2 µm/s with one integration every 0.262 seconds. Pb isotope signal variations between integrations were severe, requiring manual correction for amplifier tau signal decay effects prior to time-resolved data analysis and processing using Iolite (v.3.65) data reduction software (Paton et al., 2011). Data were normalised to Nod-A-1 (Baker et al., 2004) as the primary reference material and the data output at the integration level for

Table 1
LA-MC-ICP-MS data of all analysed reference material presented as the average ±2s%. Data from Baker et al. (2004) and GEOREM (Jochum et al., 2005) are presented for comparison.

		$^{206}Pb/^{204}Pb$	2s%	$^{207}Pb/^{204}Pb$	2s%	$^{208}Pb/^{204}Pb$	2s%	$^{208}Pb/^{206}Pb$	2s%	$^{207}Pb/^{206}Pb$	2s%
NodP	Baker et al., 2004	18.7000	0.0323	15.6380	0.0170	38.6970	0.0216	2.06936	0.0389	0.836257	0.0365
	GeoREM	18.697-18.7081		15.629-15.638		38.669-38.699		2.06850		0.835800	
	laser ablation (n = 44)	18.7029	0.0150	15.6336	0.0115	38.6895	0.0132	2.06854	0.0073	0.835821	0.0095
JMn1	laser ablation (n = 44)	18.7579	0.0112	15.6343	0.0109	38.7244	0.0147	2.06449	0.0063	0.833423	0.0048
HRM	laser ablation (n = 69)	18.8819	0.0085	15.7019	0.0083	39.0147	0.0121	2.06640	0.0048	0.831569	0.0037

plotting as a continuous profile. Nod-P-1, JMn-1 and an in-house material (HRM) prepared from a homogenised quantity of Fe-Mn crust from Tropic Seamount, were analysed during the same sessions to validate the results by comparison to published and/or in-house results determined by solution calibration. In order to maintain consistent analytical conditions between reference materials and sample thin sections, the powdered reference materials were mixed with resin, mounted on a glass-slide and then polished to produce a flat surface for laser ablation, rather than prepared as wax-bound pressed-pellets. The latter were found to have an erratic ablation behaviour during ablation tests. During each analytical session, all uncertainties were propagated for the scatter shown by Nod-A-1. Following this, no validation materials had excess scatter within a session. Nod-P-1 produced data within the range given in the GeoRem database and close to the Baker et al. (2004) values. These, and laser-ablation values determined for JMn-1 and HRM, are contained in Table 1. Values represent the reproducibility over eight analytical sessions. This study demonstrated Nod-P-1 and JMn-1 to be more heterogeneous than HRM in their Pb-isotope composition. Both are more coarsely ground than HRM. No inter-session scatter was apparent in the HRM $^{207}Pb/^{206}Pb$ data. The long-term weighted mean of HRM was 0.8316±0.0037% (95% confidence), indicating a bias relative to solution values of 0.0138%. A total $^{207}Pb/^{206}Pb$ uncertainty of 0.015% (2σ) was therefore estimated for propagation to sample data.

To confirm that the observed cycles were not analytical artefacts, the instrument response time and wash out time were investigated to calculate the spatial resolution at which mixing can occur during laser rastering. The clear physical boundaries that result from fractures in the Fe-Mn crust and filled by epoxy resin, provided an ideal location to test the spatial resolution (Fig. 2 and 3). A drop in total ion beam signal to baseline values was observed in 2 s as the laser transitions from Fe-Mn crust to epoxy resin (Fig. 3). This implied that at a raster scan speed of 2 µm/s, mixing of Pb isotope measurements could be discriminated between end-members separated by 4 µm. This signal smoothing was therefore unlikely to affect the measured $^{207}Pb/^{206}Pb$ minima and maxima of each Fe-Mn oxide laminae, which were separated by 10–40 µm.

A 7 mm transect was analysed (125–118 mm from the top of the sample, 65.1 ± 0.7–63.0 ± 0.6 Ma Josso et al. (2019), Fig. 1 and 2), covering the whole interval of interest, whilst a smaller zone was mapped to investigate: (i) correlation with major element geochemistry; and (ii) $^{207}Pb/^{206}Pb$ lateral continuity and repeatability of the measurements (Fig. 2 and 4). The 7 mm transect was used for cyclostratigraphic analysis to investigate dominant periodicities and their origin. Data collected from desiccation fractures were omitted and the remaining data stitched back together, assuming no substantial loss of material. As part of the astrochronology data processing, the $^{207}Pb/^{206}Pb$ data were interpolated to 4 µm, detrended using a high-pass filter (preserving periods <500 kyr), and then normalised by dividing by the standard deviation. Evaluation of amplitude modulation was investigated using the TimeOpt scripts (Meyers, 2015). The complete Pb isotope data set and processing scripts are described in supplementary material and available here (DOI: https://doi.org/10.5285/7a9eb43f-a5c4-450c-9fe1-c60f2703a1d1). Band-pass filters with Hilbert transforms were used to track the principal frequencies and their amplitudes, and their statistical significance confirmed (see Supplementary Material 2).

3. Results

3.1. Pb isotope and major element variation

The $^{207}Pb/^{206}Pb$ trace has an overarching trend ranging from 0.828–0.833 (Fig. 2). It shows clear regular higher-frequency oscillations that have an amplitude of 0.12–0.18% of the $^{207}Pb/^{206}Pb$ ratio and a periodicity of 10–80 µm (Fig. 2 and 4). Additional lower frequency cycles occur at interval of about 300 µm.

High-resolution SEM elemental mapping of a laminated interval (1.25 ∗ 1.75 mm, Figs. 2 and 4, Supplementary Material 1) demonstrates the regular alternation in the concentration of major elements. The 10–80 µm thick laminae present in the backscatter electron imaging reflect the composition variation in the deposit, marked by oscillations of the Fe/Mn ratio between adjacent laminae. In this laminated interval, a positive correlation is present between high Fe/Mn ratios and the concentration of Al, Si and Ti (Supplementary Material 1). The pervasive impregnation of the

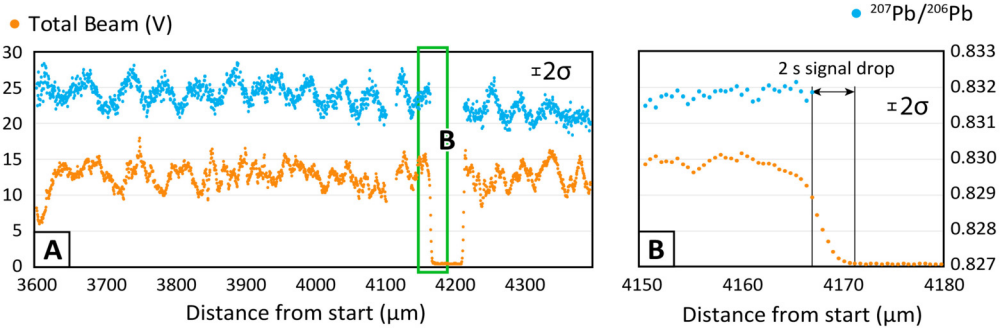

Fig. 3. (A) Extract of the $^{207}Pb/^{206}Pb$ signal shown in Fig. 2 and total beam intensity. (B) Close up of the signal decay as the laser transitions from Fe-Mn crust to epoxy resin when it crosses a fracture in the sample.

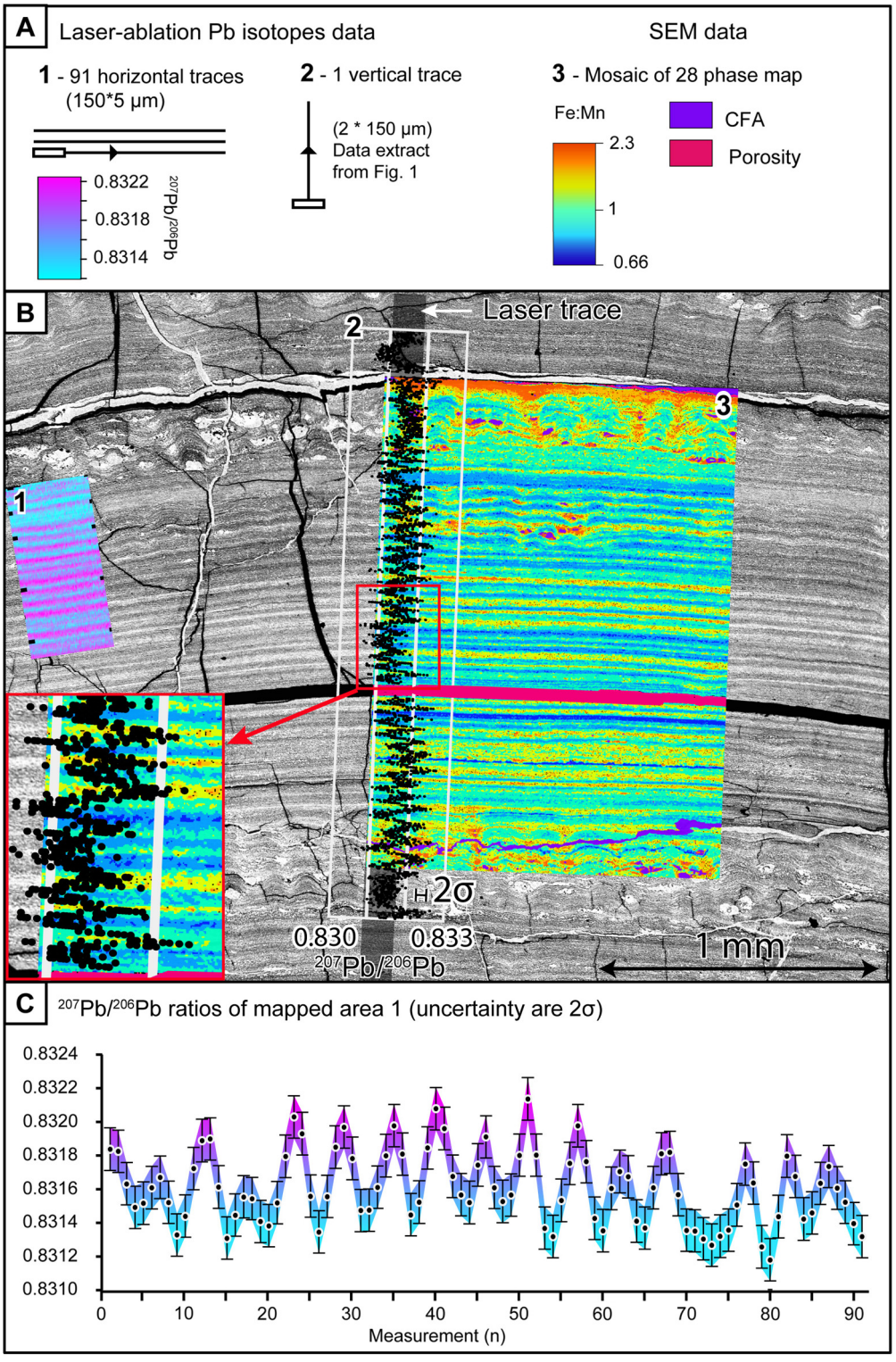

Fig. 4. (A) Details of the laser-ablation pattern that produced the Pb isotope map 1, the Pb isotope dataset used for cyclostratigraphic analysis (2) and keys to colour scale of the Pb isotope map and SEM phase mapping (map 3) in panel B. CFA = carbonate-fluoro-apatite. (B) Geochemical phase mapping and $^{207}Pb/^{206}Pb$ mapping and transect data as shown on Fig. 2. This data and the close up demonstrate the positive correlation between high Fe/Mn ratio and high $^{207}Pb/^{206}Pb$ ratio. (C) Details of the Pb isotope data produced during the 91 ablation traces used to produce map 1 using similar colour-coding.

crust by carbonate-fluoro-apatite (CFA), occurring as veinlets and small nodular masses sealing Fe-Mn oxide porosity (Josso et al., 2020b), is also clearly visible in the phase mapping data.

The high-resolution Pb isotope map (Fig. 4) also clearly shows the cyclical nature of the Pb isotope data. Map 1 represents a collation of 91 horizontal laser ablation traces ($150 * 5$ µm) running parallel to the Fe-Mn oxide layering, with 2–3 ablation traces per laminae. An extract of the whole Pb isotope transect is also presented as an overlay on the SEM backscatter image and the SEM Fe/Mn ratio map.

High-frequency cycles are also observed in the $^{208}Pb/^{206}Pb$ and $^{206}Pb/^{204}Pb$ trends (Supplementary information, DOI: https://

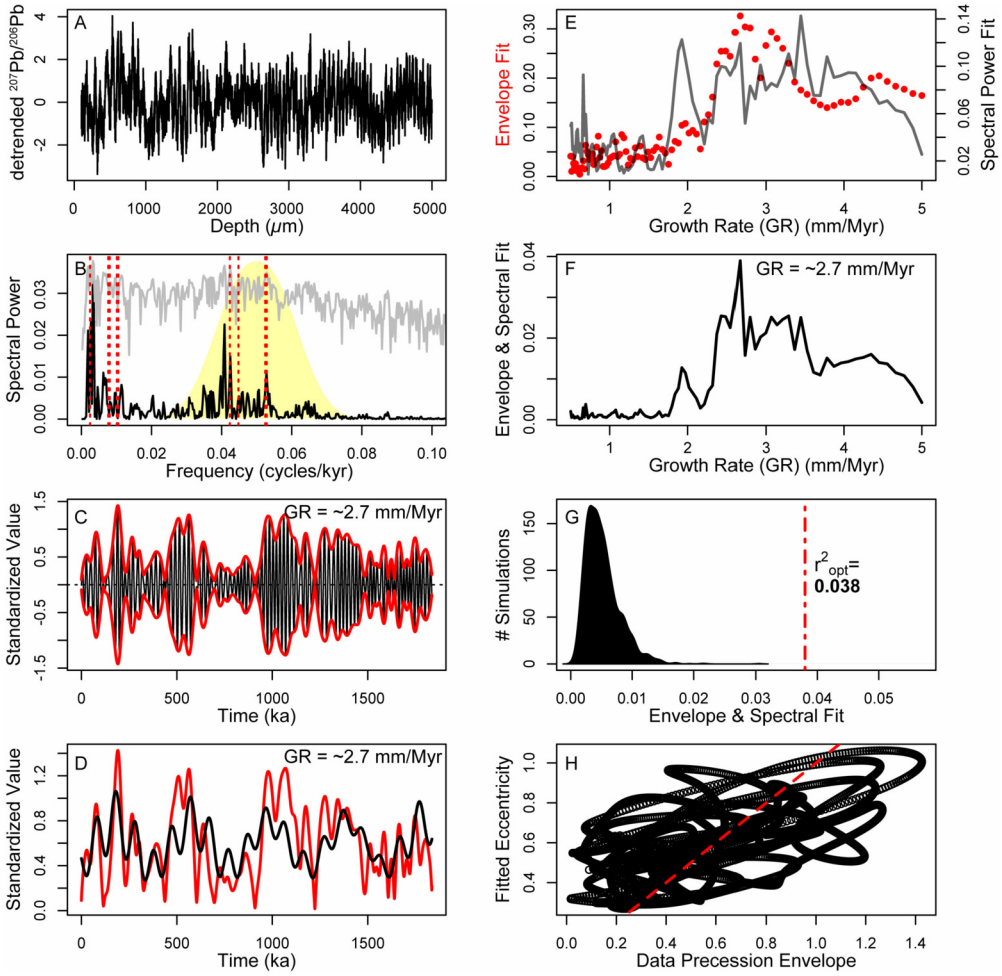

Fig. 5. TimeOpt analysis performed in Astrochron (Meyers, 2015). (A) $^{207}Pb/^{206}Pb$ processed using standard methods (see Methods) prior to cyclostratigraphic analysis. (B) Periodogram of the $^{207}Pb/^{206}Pb$ data, using the TimeOpt growth rate of 2.7 mm/Myr. Grey and black lines are log and linear spectra, respectively. Dashed red lines are the precession and eccentricity periods. Yellow shaded area in (B) has been used for band-pass filtering in (C), with instantaneous amplitude in red determined via Hilbert transform. (D) Amplitude of band-pass filtered $^{207}Pb/^{206}Pb$ (red) compared with eccentricity model reconstructed by TimeOpt (Meyers, 2015). (E) Growth rates versus resulting squared Person correlation coefficients for envelope fit (r^2, red dots) and spectral power fit (r^2, grey line), which are combined in (F). Highest r^2 fit of 0.038 is at ~2.7 mm/Myr (rounded from 2.668 mm/Myr). (G) Significance of maximum observed r^2 (from F) based on 2000 Monte Carlo simulations with AR1 surrogates ($\rho = 0.826$), yielding a p value of 0.005 (i.e., reject null hypothesis at 99.5% confidence level). (H) Cross plot of the amplitude of band-pass filtered $^{207}Pb/^{206}Pb$ and of the TimeOpt eccentricity model. Red dashed line is the 1:1 line.

doi.org/10.5285/7a9eb43f-a5c4-450c-9fe1-c60f2703a1d1). The $^{206,\,207,\,208}Pb/^{204}Pb$ ratios evolve over the stratigraphic interval considered, cycling between more radiogenic and more common Pb signatures. The $^{207,\,208}Pb/^{206}Pb$ mirror this pattern, with low $^{207,\,208}Pb/^{206}Pb$ ratio oscillations matched by radiogenic excursions in the $^{206}Pb/^{204}Pb$ domain. This suggests a dominantly uranogenic as opposed to a thorogenic source for the radiogenic Pb in this sample. Notably, average Pb concentrations of the Fe-Mn crust are 2600 ± 1000 (2σ) ppm whilst average U concentrations are 13 ± 4 (2σ) ppm (Josso et al., 2020b), excluding the possibility of in-situ radiogenic ingrowth as a source of the Pb isotope variation.

Overlaying the $^{207}Pb/^{206}Pb$ laser-ablation data on the Fe/Mn phase map highlights their synchronicity, with high Fe/Mn ratios positively correlating with higher, less radiogenic $^{207}Pb/^{206}Pb$ ratios. This correlation raises the possibility that analytical artefacts (matrix effects), related to the Fe/Mn variation could be responsible for the Pb isotope variations observed. Since Fe oxyhydroxides (rather than Mn oxides) dominantly scavenge Pb chloride and carbonate complexes in seawater during hydrogenetic precipitation (Koschinsky and Halbach, 1995), a positive correlation between Fe/Mn and the total Pb concentration would be expected. Cross-wavelet transform and squared wavelet coherence between $^{207}Pb/^{206}Pb$ and total Pb beam intensity (Supplementary Material 3) shows that these two parameters are not phase-locked, despite occasional similar periodicities, therefore ruling out a causal relationship between Pb ion beam intensity and observed oscillations in the Pb isotopic ratios. Equally, although of lower measurement precision, the total lack of $^{205}Tl/^{203}Tl$ variation or correlation with Pb isotope signature (Supplementary Material 4), is evidence against Pb isotope variations being caused by matrix changes, when Tl isotope systematics would be expected to respond in a similar way.

3.2. Age control and astronomical tuning

Due to the potential range of geologic and climatic stochastic factors that could influence the Pb isotope record, it is important to evaluate the statistical validity of these cycles compared to known astronomical changes. Cyclostratigraphic analyses using wavelets and band-pass filters (Supplementary Material 2 and 5) indicate statistically significant (at 95% confidence level), high-frequency variability with periods of 60–80 μm in the lower 2000 μm of the record, and a transient decrease to lower periods of 30–50 μm between 3000–5000 μm. In the lower half of the record (especially visible between ~400–1000 μm), a cycle with a period of about

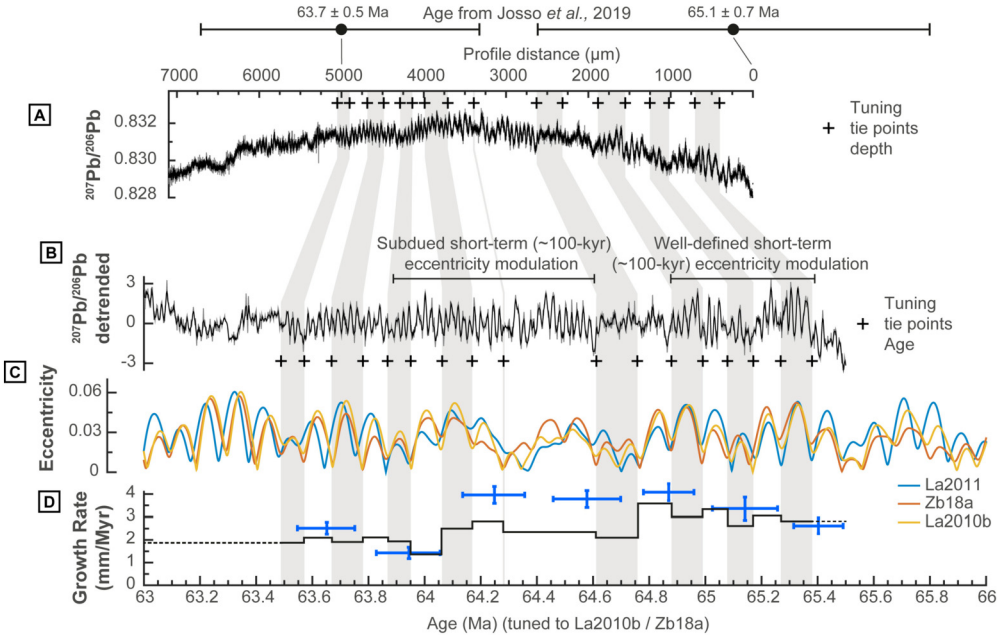

Fig. 6. Astronomical tuning of the $^{207}Pb/^{206}Pb$ data. (A) Original $^{207}Pb/^{206}Pb$ isotope data (Fig. 2), with pluses denoting age correlation points and ages for profile distance d = 0 µm and d = 5000 µm from Josso et al. (2019). (B) Detrended and normalised $^{207}Pb/^{206}Pb$ data with equal age spacing (see Methods) to emphasise the cyclicity with pluses denoting tuning tie points. (C) Astronomical solutions of Earth's eccentricity: La2011 (Laskar et al., 2011), La2010b (Laskar et al., 2011), and Zb18a (Zeebe and Lourens, 2019). (D) Growth rates resulting from cyclostratigraphic analysis (black) and Co-chronometry data ($\pm 2\sigma$, in blue) for this stratigraphic interval from Josso et al. (2019), note the convergence in growth rate estimates between the two methods.

250–400 µm generally modulates this high-frequency variability, i.e. about every 5 high-frequency cycles, approximately matching the 5:1 ratio between precession and short eccentricity cycles (Laskar et al., 2004) (Supplementary Material 6).

To test whether climatic precession may drive the observed $^{207}Pb/^{206}Pb$ variability, we use the TimeOpt script (Fig. 5) (Meyers, 2015) as part of best practice methods (Sinnesael et al., 2019). The TimeOpt analysis confirms that climatic precession and eccentricity likely drive the observed cyclicity in $^{207}Pb/^{206}Pb$. This record therefore has high potential for astronomical tuning that provides complementary age control (Supplementary Material 7). The intervals of subdued precession amplitude (i.e., eccentricity minima) in the $^{207}Pb/^{206}Pb$ data set are correlated to minima in the ~100-kyr eccentricity cycle of astronomical solutions (Laskar et al., 2011; Zeebe and Lourens, 2019), guided by the available absolute age control of 65.1 ± 0.7–63.7 ± 0.5 Ma (Fig. 6) (Josso et al., 2019). This tuning based on eccentricity cycles confirms that the higher frequency cycles reflect the imprint of climatic precession (Supplementary Material 2). The absolute age control for the laminated interval (~0–5000 µm) is also improved to ~65.5–63.5 Ma (Fig. 6). Maximum age uncertainties of the tuning range between ~10 s to ~100 kyr and originate from the uncertainties in the available astronomical solutions. The accuracy of this tuning is confirmed statistically by the excellent agreement in bandpass filters with eccentricity bandwidths and the presence of significant precession cycles in wavelets (Supplementary Material 2) and also by comparing the resulting growth rates. The growth rates obtained from the tuning, i.e., 2.5–3.5 mm/Ma in the older part and 1.5–2.5 mm/Ma in the younger part, are highly comparable to those independently obtained from Co-chronometry (Fig. 5 and 6) (Josso et al., 2019).

The textural variations between columnar and laminar structures also match the astronomical framework, with the columnar textures (~1000, ~2200, ~3500 and ~5100 µm, Fig. 2) coinciding with long-term (~405-kyr) eccentricity minima, i.e., when seasonal extremes are absent for a long period of time. In contrast, laminated textures coincide with ~405-kyr eccentricity maxima, i.e., highest seasonality. It is notable that a columnar interval appears to be missing around 4400 µm (Fig. 2). This could be explained by stochastic phenomenon or the occurrence of a relatively high-amplitude short-term (~100-kyr) eccentricity cycle in the ~405-kyr eccentricity minimum (difficult to verify due to uncertainties in the astronomical solutions, see Supplementary Material 7). Changes in Fe-Mn oxide textures relate to the balance between varying biogenic and detrital input and the strength of the oceanic current. We hypothesise that the long-term reduction of seasonality during a long-term (~405-kyr) eccentricity minima yielded more quiescent climatic and oceanic conditions whilst favouring biological activity (Zachos et al., 2010). These conditions may have been consistent with more abundant carbonate precipitation and/or higher detrital accumulation resulting in the formation of more columnar textures (Josso et al., 2020b).

4. Discussion

4.1. Mechanisms for varying Pb isotope signatures in Fe-Mn crusts

Independent dating techniques and statistical analysis indicate these Pb isotope oscillations reflect changes in the climatic precession cycle and are most likely associated with changes in the amount of major and trace elements entering the marine environment. In Pb-Pb space, the complete Pb isotope dataset plots along a single array with each high-frequency oscillation located within the same trend (Fig. 7). Therefore, the single array formed by the data can be explained in terms of simple binary mixing, reflecting varying proportions of each Pb endmember.

Pb isotope variations in the ocean as recorded by Fe-Mn crusts relate to changes in the intensity and provenance of the Pb inputs (riverine, hydrothermal, aeolian), or in response to changes in oceanic circulation pattern following opening or closing of gateways leading to the mixing of various endmembers. A change in the radiogenic isotope signature of a water mass can only occur by addition from a reservoir with a different isotopic composition, as Pb isotopes are free from fractionation induced by temperature, evaporation and biological processes (Frank et al., 2002). From

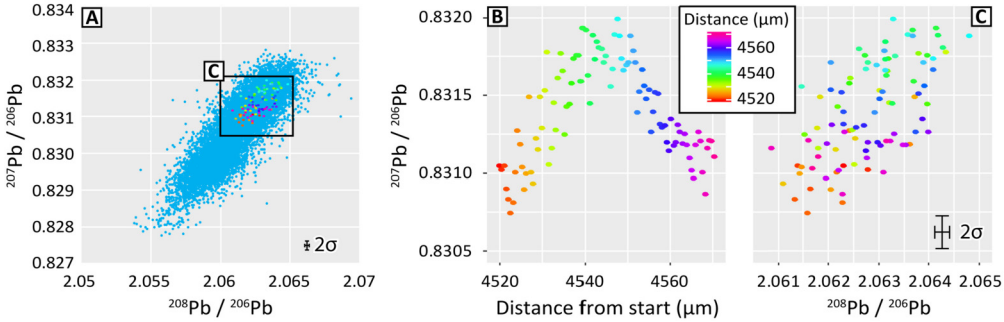

Fig. 7. (A) ^{208}Pb/^{206}Pb vs. ^{207}Pb/^{206}Pb plot of the entire transect. Note how the data plot along a single trend suggesting simple binary mixing. (B) Extract of a single ^{207}Pb/^{206}Pb oscillation, colour coded as a function of distance in the record (Fig. 2). (C) Spread of the single oscillation in Pb-Pb space (duplicated in panel A). The similar slope between the whole transect and each oscillation indicates that a two end-member mixing regime is likely to be responsible for the long- and short-term Pb isotope variations in this record.

this perspective, the early Paleocene was a relatively stable period of oceanic circulation in the North Atlantic with no significant opening or closing of oceanic seaways (Batenburg et al., 2018). The dominant source of deep-water formation was the southern region of the South Atlantic basin and northward flowing Southern Component Water filled most of the Atlantic basins (Thomas and Via, 2006; Batenburg et al., 2018). It is therefore unlikely that the signal was produced by the relative mixing of two seawater masses with different isotopic compositions following a sudden influx of exotic water. Such a process was notably observed in Fe-Mn crusts proximal to the Drake Passage, the Isthmus of Panama or the Gibraltar straight (Abouchami et al., 1999; Frank et al., 1999). Furthermore, such tectonic restructuring usually triggers regional scale reorganisation of the oceanic currents with a pronounced change in the isotopic signature, which would be hard to reconcile with the repetitive high-frequency oscillation of the record.

A potential hydrothermal or volcanic source for Pb in this record, whether proximal or distal within the Saharan Seamount Province (SSP) is unlikely. Eruption of the North Atlantic large igneous province had not initiated yet (60.5–54.5 Ma) (Jolley and Bell, 2002) whilst the only volcanic activity in the SSP within the period relevant here was the formation of the Essaouira Seamount (Van Den Bogaard, 2013), 1200 km north-east of Tropic Seamount. It is unlikely that this volcanic activity or any other hydrothermal activity in the SSP was sustained so continuously over more than 2 Ma. Although, major climatic events such as glacial-interglacial transitions may influence the volume of seawater and therefore the hydrostatic pressure on the global volcanic and hydrothermal activity at mid-oceanic ridges (Lund et al., 2016), such a mechanism is hard to reconcile with astronomically-induced major sea-level changes in an ice-free period.

However, Pb isotope records from North Atlantic Fe-Mn crusts do show a strong response to the Northern Hemisphere glaciation, which caused significant weathering of the Canadian and Scandinavian shield areas, resulting in the input of large amount of radiogenic material to the North Atlantic Deep Water (Burton et al., 1997; Abouchami et al., 1999; Foster and Vance, 2006). This suggests that the Pb isotope signature of seawater precipitates is dominantly influenced by local weathering and erosional factors. Accordingly, the most likely explanation for the Pb isotope variations observed in this record is changing contributions from the continental endmember. Tropic Seamount is located 450 km off the coast of West Africa, halfway between the Canary Islands and Cape Verde Islands. It lies in one of the main drainage regions for the Precambrian West African Craton (WAC), Hercynian collision belts and the Neoproterozoic sedimentary sequences of West Africa (Fig. 8). Given this mixture of cratonic and sedimentary terranes, it is likely that the oscillations observed in the Fe-Mn crust reflect a change in the influence of one or more geological components from western Africa. Pb isotope variations in seawater can result from varying proportions of input from multiple sources with distinct signatures, but also as a result of the incongruent release of Pb during weathering of a single end-member. During the early stages of continental weathering, preferential dissolution of U-containing accessory phases (allanite, monazite, titanite, apatite) releases more radiogenic Pb than represented by the bulk parent rock (Harlavan and Erel, 2002). The older the rock, the more radiogenic this signature. This was previously highlighted as the reason for glacial-interglacial Pb isotopic variations in North Atlantic Fe-Mn crusts and attributed to enhanced chemical weathering of old Canadian terranes under warmer and wetter temperatures during interglacial periods, which imparted a more radiogenic signature to the adjacent seawater (Foster and Vance, 2006). In contrast, during glacial periods physical weathering predominates, resulting in a Pb isotopic signature more reflective of the whole rock composition. To explore the role played by each weathering mechanism in the formation of the Pb isotope record obtained from Tropic Seamount, it is first necessary to understand the climatic regime influencing the study area during the Paleocene.

4.2. Climate implications

Africa's modern-day tropical climate is characterised by the annual alternation of semi-arid conditions and monsoonal precipitation around the equatorial belt. This is the manifestation of seasonal migration of the Inter-Tropical Convergence Zone (ITCZ), the longitudinal corridor where trade winds from the two hemispheres converge (Nicholson, 2009). This effects the position of the tropical rain belt, which naturally follows insolation, migrating northward in the boreal summer and southward in the austral summer (Nicholson, 2009).

Numerous climate models show that over the course of climatic precession cycles, stronger boreal insolation results in an increase in summer temperatures over northern Africa, leading to a meridional pressure gradient, enhanced moisture transport from the Atlantic Ocean towards North Africa, and increased precipitation in the region (Demenocal and Tierney, 2012; Prömmel et al., 2013). Consequently, insolation directly influences the intensity and extent of northward migration of the tropical rain belt. It is estimated that a 7% increase in solar radiation over a climatic precession cycle could result in a 17–50% increase in African monsoonal rainfall (Demenocal and Tierney, 2012).

There is considerable evidence that the geological record of tropical Africa has been sensitive to precessional variability in insolation, causing changes in wind patterns, precipitation, and net freshwater flux (Kuechler et al., 2013). This is largely recognised in the recent (<2 Ma) African climate whereby latitudinal changes in the position of the ITCZ influenced the proportion of dust, pollen

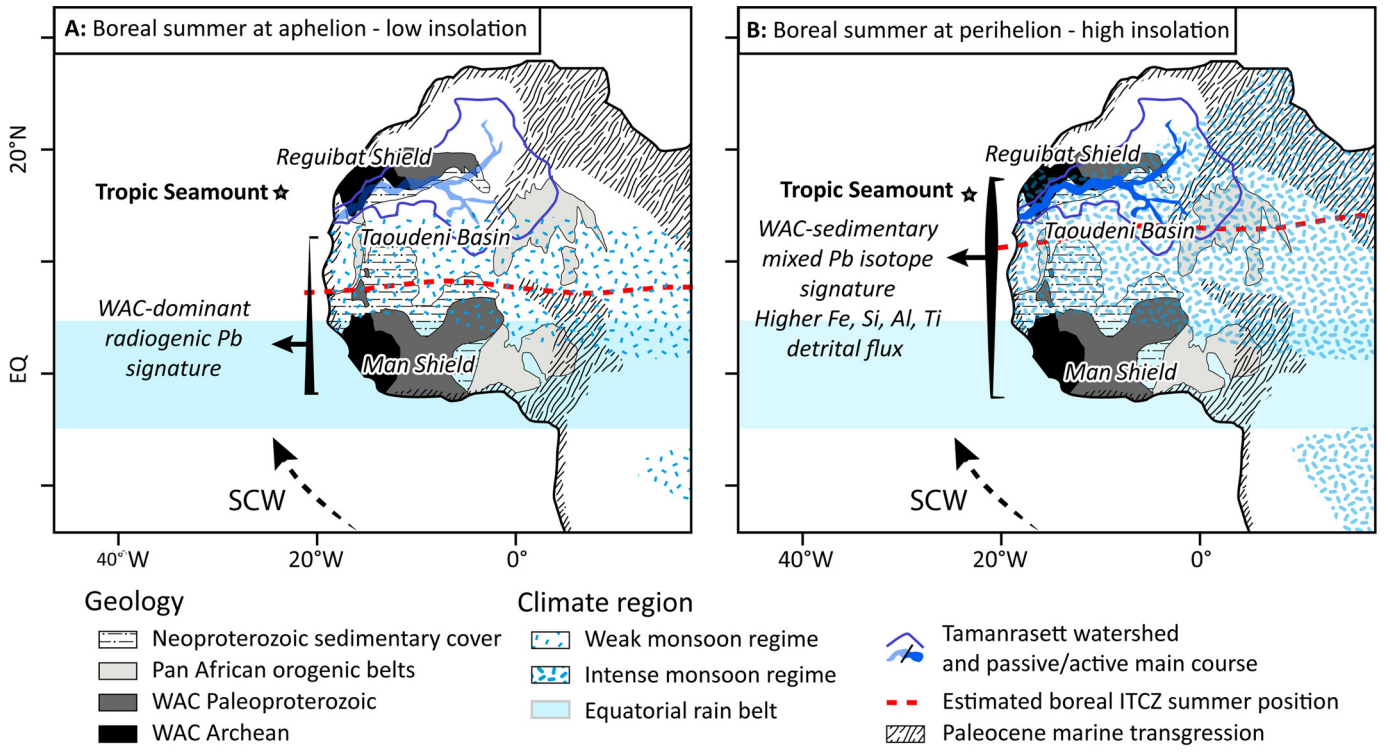

Fig. 8. Model illustrating the impact of climatic precession on insolation, the distribution and intensity of monsoonal rainfall over West Africa during the Paleocene, and the resulting Pb isotope and detrital contributions to the north-east Atlantic Basin. The Tamanrasett watershed and main course are based on Skonieczny et al. (2015), the extent of paleo monsoonal region in the Paleocene is based on Liu et al. (2019), whilst the paleo-shoreline for the Paleocene marine transgression is after Luger (2003). WAC = West African Craton, SCW = Southern Component Water.

and other biomarkers in lake records in tune with astronomical parameters (Kuechler et al., 2013). Similarly, marine records proximal to the Congo River and Sierra Leone Rise demonstrate the influence of astronomical forcing on the flux, source and provenance of the terrigenous inputs in these basins during both the Pleistocene and Cretaceous (Abouchami and Zabel, 2003; Beckmann et al., 2005).

Although no major river system currently drains the Western Sahara, this region experienced recurrent humid episodes in the late Quaternary, associated with the development of vast fluvial networks. The presence of large erosive submarine canyons and fluvial sediments on the western African margin, such as the Cape Timiris Canyon, and identification of large paleodrainage networks; e.g. the Tamanrasett watershed, buried under recent sediments, support the idea that large volumes of discharge occurred during African humid periods (Skonieczny et al., 2015). Based on this interpretation, the extended Tamanrasett watershed drained the southern Atlas, the western portion of the Hoggar Mountains, currently in south-east Algeria, and a major portion of the Taoudeni sedimentary basin. The African Humid Period was concurrent with the northernmost position of the tropical rain belt during high boreal insolation periods (Fig. 8) (Tierney et al., 2011; Skonieczny et al., 2015).

Older proxy records of C and O isotopes, aeolian sedimentation and palynological studies indicate that a greater proportion of Africa had a humid climate and was covered by extensive woodlands and forests, in contrast to the arid and semi-arid conditions that prevail today (Bobe, 2006). Although the Paleocene and Eocene were the warmest periods in the Cenozoic, this did not result in arid or desert conditions as Africa was bathed to the north and east by the shallowing Tethys seaway. Notably, the Paleocene shoreline extended far in-land over most of North Africa and Gulf of Guinea (Fig. 8, Luger (2003)). Warm oceanic conditions lead to abundant atmospheric moisture and high precipitation on the continent (Zachos et al., 2001; Bobe, 2006).

Furthermore, the African continent migrated northward by 8–10° over the last 65 Ma (Van Hinsbergen et al., 2015). As a result, in the Early Paleocene, the equatorial rain belt was located over most of the southern part of western Africa. The tropical rain belt and monsoons extended as far north as the southern edge of the current location of the Atlas mountains during high boreal insolation periods (Fig. 8) (Liu et al., 2019). It is therefore plausible that the (paleo)Tamanrasett drainage network was active in the Paleocene, either permanently or temporally, with potentially high quantities of freshwater run-off augmented by monsoonal precipitation.

For these reasons, it is considered that rivers were the dominant vector for the transport of Pb from West Africa to the ocean during the Paleocene and that incongruent weathering is unlikely to play a major role in changing contributions from the continent. Although Saharan dust currently plays a major role in the budget and fertilisation of the Atlantic Ocean, it is unlikely aerosols were abundant in the Paleocene given the warmer climate, high precipitation, vegetation, and presence of shallow seas covering most of the current dust source areas (Luger, 2003). Earliest evidence for the aridification of North Africa are dated to the Tortonian (11.6–7.2 Ma) (Zhang et al., 2014; Herbert et al., 2016).

4.3. Conceptual model

Given this climatic context, the contribution of the different western African source rocks to the average Pb isotope signature being transported to the north-east Atlantic can be summarised as follows:

- The exposed shield areas of the West African Craton; the Reguibat and Man Shield (Fig. 8), have a similar structure formed by a collage of Archean granitic terranes in the west and Paleoproterozoic high-grade metamorphic terranes in the

east (Fig. 8, Schofield et al. (2012)). Given the Precambrian age and petrology of these terranes, they represent the most radiogenic endmember of West African geology.

- The Taoudeni Basin formed following subsidence and stabilisation of the Precambrian cratonic units about 1700 Ma ago (Rooney et al., 2010). This >2000 m thick sedimentary succession comprises Proterozoic to Paleozoic rocks derived from cratonic erosion and subsequent deposition in shallow to deep marine environments (Kah et al., 2012). Thin Mesozoic to Cenozoic age rocks cover the basin towards its centre, whilst large areas are covered by Quaternary sand dunes. Sedimentary units from the Taoudeni Basin are likely to have a less radiogenic isotopic signature than the igneous and metamorphic Precambrian basement, and are closer in composition to the common Pb endmember of the dataset presented here.

Considering the paleogeographic and climatic reconstructions, the average Pb isotope composition of the weathering of West Africa represents a mixture between the continuously weathered Precambrian Man Shield under equatorial conditions, and varying contributions from the younger Pan African belt and Taoudeni Basin, as a function of monsoonal rainfall impacted by precession (Fig. 8). Therefore, during periods of high boreal insolation, more intense monsoons, which covered a larger geographical area, increased the contribution of sedimentary material from the Taoudeni Basin to the north-east Atlantic, imparting a less radiogenic isotope signature to the seawater. Whilst under these conditions a larger Pb contribution from the Reguibat Shield would be expected and be similar to that of the Man Shield, it would remain a minor component relative to the total Pb flux from the Neoproterozoic and Palaeozoic sequences of the Taoudeni Basin.

In addition, this model provides a consistent explanation for the observed co-variation between Pb isotopes and major element variations in each lamination of the Fe-Mn crust sample. The elemental and isotopic mapping of the laminated section (Fig. 4, Supplementary Material 1) demonstrates that the least radiogenic Pb signature (low $^{206}Pb/^{204}Pb$ and high $^{207,208}Pb/^{206}Pb$), is associated with laminations that have high Fe/Mn ratios, and high Al, P, Si, Ti (Supplementary Material 1), which correspond to periods of high insolation based on the model outlined above. During the precipitation of Fe and Mn oxide colloids in seawater, these particles possess opposite surface charge and will, therefore, scavenge dominantly anions and neutrally surface-charged particles or cations, respectively. The observed geochemical correlation between Fe and Al, Si, P and Ti follows this simple electrostatic scavenging model as Ti, Al and Si are largely present in seawater as neutral hydroxides ($Al(OH)_3$, $Si(OH)_4$, $Ti(OH)_4$), whilst P is mostly present as HPO_4^{2-} (Koschinsky and Halbach, 1995; Lusty et al., 2018). Iron is 40–60 times more abundant than Mn in the Earth's crust. Therefore, more intense precipitation over a larger portion of the Tamanrasett watershed during periods of high insolation would have led to the release of a larger amount of dissolved and particulate Fe into watercourses and seawater. Furthermore, given the dominant siliciclastic nature of the rocks of the Taoudeni Basin, the enhanced contribution from this endmember would also contributed additional Si, Al and Ti to seawater that has a more common Pb isotopic signature.

4.4. Mass balance calculation

The contribution from each endmember between precession maxima and minima is calculated using a simple mass balance calculation (Fig. 9). There is an absence of relevant Pb isotope data for the rock formations from this region. Therefore, Pb isotope data for river water and sediments data from the Niger and Congo rivers provides the best estimates of the range of Pb values entering the Atlantic Ocean that are derived from these terranes (Allègre et al., 1996; Frank et al., 2003; Millot et al., 2004) (Fig. 8 and 9). The Fe-Mn crust data plot in the middle of the range of reported values for the Congo tributaries that are draining mixed Precambrian cratonic units and Mesozoic sedimentary formations. These are a good analogue for the Man shield, Reguibat Shield and Taoudeni Basin of the West African Craton. The maximum amplitude of variation observed in the Pb isotope record during a half-precession cycle is 0.0017 in $^{207}Pb/^{206}Pb$ composition, and this varies from 0.8306 to 0.8289 near the base of the record (Fig. 2). Using the two extreme compositional values of the Congo tributaries (0.802–0.863) as endmembers and assuming constant weathering rates and equivalent Pb concentrations between the two endmembers given extreme dilution by seawater, a relative contribution change of ±2.8% of the less radiogenic endmember is required to explain the maximal variation observed in the Pb isotope data. Rainfall can be 17–50% higher during a climatic precession maximum compared to a minimum. Given the northern migration of the ITCZ during periods of high insolation, more intense monsoonal conditions cover/effect larger areas of sedimentary rocks relative to the constant weathering of cratonic shield units in the equatorial rain belt. Given the broad assumptions made for these calculations, this relative change in contribution seems plausible with the climatic reconstructions and rainfall variability between the two extremes.

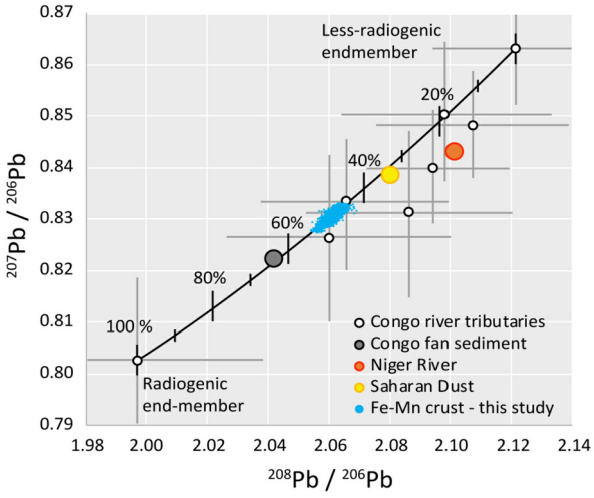

Fig. 9. $^{208}Pb/^{206}Pb$ vs $^{207}Pb/^{206}Pb$ plot of the Niger (Millot et al., 2004) and Congo fan sediments (Frank et al., 2003), suspended sediments from the Congo River tributaries (Allègre et al., 1996), Saharan dust (Abouchami and Zabel, 2003) and Fe-Mn crust LA-MC-ICP-MS Pb data produced in this study. Owing to their broadly similar geological formations, data from the Congo River tributaries are considered to reflect the composition of the potential extreme Pb end-members resulting from drainage of the Man Shield, Reguibat Shield and Taoudeni Basin towards the north-east Atlantic. The solid line represents the mixing trend between the two end-members assuming equal Pb concentrations.

5. Applications and conclusions

Frequency analysis of high-spatial resolution LA-MC-ICP-MS Pb isotope data measured in an Fe-Mn crust highlights the presence of ~20, ~100 and ~405 ka cycles, representing the effect of astronomical precession with eccentricity modulation. This cyclostratigraphic analysis yields growth rates of 1.5–3.5 mm/Ma consistent with previous estimates from Co-chronometry for this stratigraphic interval.

The isotopic and major element variations observed in this Fe-Mn crust have been successfully correlated to periodic variation in the intensity and geographic extent of the tropical rain belt, which

is controlled by periods of precessional high and low insolation in the Northern Hemisphere.

This study represents the first time a precession signal has been identified with high statistical significance in oceanic Fe-Mn crusts. The use of LA-MC-ICP-MS for the production of high-resolution Pb isotope data opens up new opportunities for tracing the development of these archives on astronomical time-scales. Indeed, given the 4 µm spatial resolution of the Pb isotope data and cycles of ~20 ka occurring over 40–80 µm, the temporal resolution achieved in this study ranges from 1000–2000 years. It therefore provides a powerful new tool for complementary, high-resolution dating of Fe-Mn crust sections. It also opens up the possibility of evaluating the precision and accuracy of the varied Fe-Mn crust dating techniques, by comparing the cyclostratigraphy of a recent portion of crust (<10 Ma) with its equivalent ^{10}Be chronology, Th excess dating and Co chronometry. As was necessary for this study, such comparisons would require samples in which the recent growth of Fe-Mn forms well defined laminations to provide good stratigraphic control on the data acquired and its spatial-temporal resolution. Whilst Fe-Mn crusts are generally considered to be important long-term records of seawater isotopic and compositional trends, the findings of this study suggest there are many new opportunities for high temporal resolution paleoceanographic reconstruction using this approach.

CRediT authorship contribution statement

Pierre Josso: Conceptualization, Formal analysis, Investigation, Methodology, Validation, Visualization, Writing - original draft, Writing - review & editing. **Tim van Peer:** Formal analysis, Methodology, Software, Visualization, Writing - original draft, Writing - review & editing. **Matthew S.A. Horstwood:** Formal analysis, Methodology, Validation, Writing - review & editing. **Paul Lusty:** Conceptualization, Funding acquisition, Project administration, Supervision, Writing - review & editing. **Bramley Murton:** Conceptualization, Funding acquisition, Project administration, Supervision, Writing - review & editing.

Declaration of competing interest

The authors declare no conflict of interest.

Acknowledgements

PJ, MH and PL publish with the permission of the Executive Director, British Geological Survey (UKRI). This research was supported by Natural Environmental Research Council (NERC) grants NE/M011186/1 (awarded to B. Murton) and NE/M011151/1 (awarded to P. Lusty), which fund the MarineE-Tech project. The authors gratefully thank the reviewers for their comments and suggestions that greatly improved the impact of the manuscript and the team involved in the RRS James Cook JC142 expedition to Tropic Seamount in 2016. All relevant data to this publication can be access through the British Geological Survey National Geoscience Data Centre (NGDC): DOI https://doi.org/10.5285/7a9eb43f-a5c4-450c-9fe1-c60f2703a1d1.

Appendix A. Supplementary material

Supplementary material related to this article can be found online at https://doi.org/10.1016/j.epsl.2020.116651.

References

Abouchami, W., Goldstein, S.L., Gazer, S.J.G., Eisenhauer, A., Mangini, A., 1997. Secular changes of lead and neodymium in central Pacific seawater recorded by a Fe-Mn crust. Geochim. Cosmochim. Acta 61, 3957–3974.

Abouchami, W., Galer, S.J.G., Koschinsky, A., 1999. Pb and Nd isotopes in NE Atlantic Fe–Mn crusts: proxies for trace metal paleosources and paleocean circulation. Geochim. Cosmochim. Acta 63, 1489–1505.

Abouchami, W., Zabel, M., 2003. Climate forcing of the Pb isotope record of terrigenous input into the Equatorial Atlantic. Earth Planet. Sci. Lett. 213, 221–234.

Allègre, C.J., Dupré, B., Négrel, P., Gaillardet, J., 1996. Sr·Nd·Pb isotope systematics in Amazon and Congo River systems: constraints about erosion processes. Chem. Geol. 131, 93–112.

Baker, J., Peate, D., Waight, T., Meyzen, C., 2004. Pb isotopic analysis of standards and samples using a 207Pb–204Pb double spike and thallium to correct for mass bias with a double-focusing MC-ICP-MS. Chem. Geol. 211, 275–303.

Batenburg, S.J., Voigt, S., Friedrich, O., Osborne, A.H., Bornemann, A., Klein, T., Pérez-Díaz, L., Frank, M., 2018. Major intensification of Atlantic overturning circulation at the onset of Paleogene greenhouse warmth. Nat. Commun. 9, 4954.

Beckmann, B., Flögel, S., Hofmann, P., Schulz, M., Wagner, T., 2005. Orbital forcing of Cretaceous river discharge in tropical Africa and ocean response. Nature 437, 241–244.

Bobe, R., 2006. The evolution of arid ecosystems in eastern Africa. J. Arid Environ. 66, 564–584.

Bonnefille, R., 2010. Cenozoic vegetation, climate changes and hominid evolution in tropical Africa. Glob. Planet. Change 72, 390–411.

Burton, K.W., Ling, H.-F., O'nions, R.K., 1997. Closure of the Central American Isthmus and its effect on deep-water formation in the North Atlantic. Nature 386, 382.

Christensen, J.N., Halliday, A.N., Godfrey, L.V., Hein, J.R., Rea, D.K., 1997. Climate and ocean dynamics and the lead isotopic records in Pacific ferromanganese crusts. Science 277, 913–918.

Demenocal, P.B., Tierney, J.E., 2012. African humid periods paced by Earth's orbital changes. Nat. Educ. Knowl. 3 (10), 12.

Foster, G.L., Vance, D., 2006. Negligible glacial–interglacial variation in continental chemical weathering rates. Nature 444, 918.

Frank, M., O'nions, R.K., Hein, J.R., Banakar, V.K., 1999. 60 Myr records of major elements and Pb-Nd isotopes from hydrogenous ferromanganese crusts: reconstruction of seawater paleochemistry. Geochim. Cosmochim. Acta 63, 1689–1708.

Frank, M., Whiteley, N., Kasten, S., Hein, J.R., O'nions, K., 2002. North Atlantic Deep Water export to the Southern Ocean over the past 14 Myr: Evidence from Nd and Pb isotopes in ferromanganese crusts. Paleoceanography 17, 12-1–12-9.

Frank, M., Van De Flierdt, T., Halliday, A.N., Kubik, P.W., Hattendorf, B., Günther, D., 2003. Evolution of deepwater mixing and weathering inputs in the central Atlantic Ocean over the past 33 Myr. Paleoceanography 18.

Gutjahr, M., Frank, M., Halliday, A.N., Keigwin, L.D., 2009. Retreat of the Laurentide ice sheet tracked by the isotopic composition of Pb in western North Atlantic seawater during termination 1. Earth Planet. Sci. Lett. 286, 546–555.

Han, X., Jin, X., Yang, S., Fietzke, J., Eisenhauer, A., 2003. Rhythmic growth of Pacific ferromanganese nodules and their Milankovitch climatic origin. Earth Planet. Sci. Lett. 211, 143–157.

Harlavan, Y., Erel, Y., 2002. The release of Pb and REE from granitoids by the dissolution of accessory phases. Geochim. Cosmochim. Acta 66, 837–848.

Herbert, T.D., Lawrence, K.T., Tzanova, A., Peterson, L.C., Caballero-Gill, R., Kelly, C.S., 2016. Late Miocene global cooling and the rise of modern ecosystems. Nat. Geosci. 9, 843–847.

Jochum, K.P., Nohl, U., Herwig, K., Lammel, E., Stoll, B., Horfmann, A., 2005. Geostandards and Geoanalytical Research.

Jolley, D.W., Bell, B.R., 2002. The evolution of the North Atlantic Igneous Province and the opening of the NE Atlantic rift. Geol. Soc. (Lond.) Spec. Publ. 197, 1–13.

Josso, P., Parkinson, I., Horstwood, M., Lusty, P., Chenery, S., Murton, B., 2019. Improving confidence in ferromanganese crust age models: a composite geochemical approach. Chem. Geol. 513, 108–119.

Josso, P., Horstwood, M.S.A., Millar, I.L., Pashley, V., Lusty, P.A.J., Murton, B., 2020a. Development of a correlated Fe-Mn crust stratigraphy using Pb and Nd isotopes and its application to paleoceanographic reconstruction in the Atlantic. Paleoceanogr. Paleoclimatol. 35, e2020PA003928.

Josso, P., Rushton, J., Lusty, P., Matthews, A., Chenery, S., Holwell, D., Kemp, S.J., Murton, B., 2020b. Late Cretaceous and Cenozoic paleoceanography from north-east Atlantic ferromanganese crust microstratigraphy. Mar. Geol. 422, 106122.

Kah, L.C., Bartley, J.K., Teal, D.A., 2012. Chemostratigraphy of the Late Mesoproterozoic Atar Group, Taoudeni Basin, Mauritania: Muted isotopic variability, facies correlation, and global isotopic trends. Precambrian Res. 200–203, 82–103.

Koschinsky, A., Halbach, P., 1995. Sequential leaching of marine ferromanganese precipitates: genetic implications. Geochim. Cosmochim. Acta 59, 5113–5132.

Koschinsky, A., Hein, J.R., 2017. Marine ferromanganese encrustations: archives of changing oceans. Elements 13 (3), 177–182.

Kuechler, R.R., Schefuß, E., Beckmann, B., Dupont, L., Wefer, G., 2013. NW African hydrology and vegetation during the Last Glacial cycle reflected in plant-wax-specific hydrogen and carbon isotopes. Quat. Sci. Rev. 82, 56–67.

Laskar, J., Robutel, P., Joutel, F., Gastineau, M., Correia, A.C.M., Levrard, B., 2004. A long-term numerical solution for the insolation quantities of the Earth. Astron. Astrophys. 428, 261–285.

Laskar, J., Fienga, A., Gastineau, M., Manche, H., 2011. La2010: a new orbital solution for the long-term motion of the Earth. Astron. Astrophys. 532.

Liu, X., Dong, B., Yin, Z.-Y., Smith, R.S., Guo, Q., 2019. Continental drift, plateau uplift, and the evolutions of monsoon and arid regions in Asia, Africa, and Australia during the Cenozoic. Sci. China Earth Sci. 62, 1053–1075.

Luger, P., 2003. Paleobiogeography of late Early Cretaceous to Early Paleocene marine Ostracoda in Arabia and North to Equatorial Africa. Palaeogeogr. Palaeoclimatol. Palaeoecol. 196, 319–342.

Lund, D.C., Asimow, P.D., Farley, K.A., Rooney, T.O., Seeley, E., Jackson, E.W., Durham, Z.M., 2016. Enhanced East Pacific Rise hydrothermal activity during the last two glacial terminations. Science 351, 478–482.

Lusty, P., Hein, J.R., Josso, P., 2018. Formation and occurrence of ferromanganese crusts: Earth's storehouse for critical metals. Elements 14, 313–318.

Meyers, S.R., 2015. The evaluation of eccentricity-related amplitude modulation and bundling in paleoclimate data: an inverse approach for astrochronologic testing and time scale optimization. Paleoceanography 30, 1625–1640.

Millot, R., Allègre, C.-J., Gaillardet, J., Roy, S., 2004. Lead isotopic systematics of major river sediments: a new estimate of the Pb isotopic composition of the Upper Continental Crust. Chem. Geol. 203, 75–90.

Mizell, K., Hein, J.R., Lam, P.J., Koppers, A.a.P., Staudigel, H., 2020. Geographic and oceanographic influences on ferromanganese crust composition along a Pacific Ocean meridional transect, 14 N to 14S. Geochem. Geophys. Geosyst. 21, e2019GC008716.

Nicholson, S.E., 2009. A revised picture of the structure of the "monsoon" and land ITCZ over West Africa. Clim. Dyn. 32, 1155–1171.

Paton, C., Hellstrom, J., Paul, B., Woodhead, J., Hergt, J., 2011. Iolite: freeware for the visualisation and processing of mass spectrometric data. J. Anal. At. Spectrom. 26, 2508–2518.

Prömmel, K., Cubasch, U., Kaspar, F., 2013. A regional climate model study of the impact of tectonic and orbital forcing on African precipitation and vegetation. Palaeogeogr. Palaeoclimatol. Palaeoecol. 369, 154–162.

Reynolds, B.C., Frank, M., O'nions, R.K., 1999. Nd- and Pb-isotope time series from Atlantic ferromanganese crusts: implications for changes in provenance and paleocirculation over the last 8 Myr. Earth Planet. Sci. Lett. 173, 381–396.

Rooney, A.D., Selby, D., Houzay, J.-P., Renne, P.R., 2010. Re–Os geochronology of a Mesoproterozoic sedimentary succession, Taoudeni basin, Mauritania: implications for basin-wide correlations and Re–Os organic-rich sediments systematics. Earth Planet. Sci. Lett. 289, 486–496.

Schofield, D.I., Horstwood, M.S.A., Pitfield, P.E.J., Gillespie, M., Darbyshire, F., O'connor, E.A., Abdouloye, T.B., 2012. U–Pb dating and Sm–Nd isotopic analysis of granitic rocks from the Tiris Complex: new constraints on key events in the evolution of the Reguibat Shield, Mauritania. Precambrian Res. 204–205, 1–11.

Sinnesael, M., De Vleeschouwer, D., Zeeden, C., Batenburg, S.J., Da Silva, A.C., De Winter, N.J., Dinarès-Turell, J., Drury, A.J., Gambacorta, G., Hilgen, F.J., Hinnov, L.A., Hudson, A.J.L., Kemp, D.B., Lantink, M.L., Laurin, J., Li, M., Liebrand, D., Ma, C., Meyers, S.R., Monkenbusch, J., Montanari, A., Nohl, T., Pälike, H., Pas, D., Ruhl, M., Thibault, N., Vahlenkamp, M., Valero, L., Wouters, S., Wu, H., Claeys, P., 2019. The Cyclostratigraphy Intercomparison Project (CIP): consistency, merits and pitfalls. Earth-Sci. Rev. 199, 1–16.

Skonieczny, C., Paillou, P., Bory, A., Bayon, G., Biscara, L., Crosta, X., Eynaud, F., Malaizé, B., Revel, M., Aleman, N., Barusseau, J.P., Vernet, R., Lopez, S., Grousset, F., 2015. African humid periods triggered the reactivation of a large river system in Western Sahara. Nat. Commun. 6, 8751.

Thomas, D.J., Via, R.K., 2006. Evolution of Atlantic thermohaline circulation: early oligocene onset of deep-water production in the North Atlantic. Geology 34, 441–444.

Tierney, J.E., Lewis, S.C., Cook, B.I., Legrande, A.N., Schmidt, G.A., 2011. Model, proxy and isotopic perspectives on the East African Humid Period. Earth Planet. Sci. Lett. 307, 103–112.

Van De Flierdt, T., Frank, M., Halliday, A.N., Hein, J.R., Hattendorf, B., Günther, D., Kubik, P.W., 2003. Lead isotopes in North Pacific deep water – implications for past changes in input sources and circulation patterns. Earth Planet. Sci. Lett. 209, 149–164.

Van Den Bogaard, P., 2013. The origin of the Canary Island Seamount Province - new ages of old seamounts. Sci. Rep. 3, 1–7p.

Van Hinsbergen, D.J.J., De Groot, L.V., Van Schaik, S.J., Spakman, W., Bilj, P.K., Sluijs, A., Langereis, C.G., Brinkhuis, H., 2015. A paleolatitude calculator for paleoclimate studies. PLoS ONE 10.

Zachos, J., Pagani, M., Sloan, L., Thomas, E., Billups, K., 2001. Trends, rhythms, and aberrations in global climate 65 Ma to present. Science 292, 686–693.

Zachos, J.C., Mccarren, H., Murphy, B., Röhl, U., Westerhold, T., 2010. Tempo and scale of late Paleocene and early Eocene carbon isotope cycles: implications for the origin of hyperthermals. Earth Planet. Sci. Lett. 299, 242–249.

Zeebe, R.E., Lourens, L.J., 2019. Solar system chaos and the Paleocene-Eocene boundary age constrained by geology and astronomy. Science 365, 926–929.

Zhang, Z., Ramstein, G., Schuster, M., Li, C., Contoux, C., Yan, Q., 2014. Aridification of the Sahara desert caused by Tethys Sea shrinkage during the Late Miocene. Nature 513, 401.